Wireless Cable Testing for MIMO Radios:

A Compact and Cost-effective 5G Radio Performance Test Solution

Fan, Wei; Li, Mengting; WANG, ZHENGPENG ; Zhang, Fengchun

Published in:
I E E E Transactions on Antennas and Propagation

DOI (link to publication from Publisher):
10.1109/TAP.2023.3303992

Publication date:
2023

Document Version
Accepted author manuscript, peer reviewed version

Wireless Cable Testing for MIMO Radios: A Compact and Cost-Effective 5G Radio Performance Test Solution

Wei Fan, *Senior Member, IEEE*, Mengting Li, Zhengpeng Wang, *Member, IEEE*, and Fengchun Zhang

***Abstract*— Over-the-air (OTA) radiated testing is seen as inevitable for future radio devices due to integrated transceiver radio designs. Wireless cable solution, which can achieve traditional cabled testing functionality OTA, has attracted great attention from industry, standardization, and academia in recent years for multiple-input multiple-output (MIMO) device performance testing. In state-of-the-art wireless cable solutions, the compensation of the transfer matrix between the OTA probes and antenna ports of the device under test (DUT) is implemented with the help of radio channel emulators (CEs). However, the radio CEs are not customized for such implementations, leading to expensive systems and a waste of valuable CE resources. Employing more probe antennas is a known and effective strategy to improve the robustness and quality of the wireless cable connection, which would further increase the system cost with existing implementations. To address these issues, a novel wireless cable implementation employing a stand-alone programmable amplitude and phase control network is proposed. Though simple and cost-effective, the proposed scheme is demonstrated to work in practice, and it is applicable for more generic testing scenarios where a CE is not required. The experiment validation measurements obtained in the vector network analyzer (VNA)-based passive measurement setup as well as in the active measurement setup clearly demonstrate the effectiveness and robustness of the proposed scheme.**

***Index Terms*— Antenna testing, channel emulator (CE), over-the-air (OTA) testing, radio channel, wireless cable solution.**

I. Introduction

As 5G technology matures, the time for large-scale 5G commercialization is now [1]. As the roll-out of 5G accelerates, testing, validation, and optimization of 5G radio devices are important to ensure that the 5G device should perform the way it is intended to [2]. Without rigorous testing, a device can perform poorly or fail to work. Testing is required in the stage of research and development and production. For example, conformance testing, which has been specified in standard technical specifications, is a critical milestone that all base stations (BSs) and user equipments (UEs) must pass before being released into the market [1], [3], [4], [5].

One essential step is to validate 5G radio performance under typical deployment scenarios (i.e., in realistic propagation channels) in the laboratory conditions. Cabled tests have been dominantly used to measure performance for 4G long-term-evolution (LTE) as well as 5G new radio (NR) at a frequency range (FR) 1 (which covers a FR from 410 to 7125 MHz). With cabled tests, radio frequency (RF) coaxial cables are used as the interface between the device under test (DUT) antenna ports and testing instrument ports. By doing so, desired testing signals can be faithfully guided to respective antenna ports on the DUT without distortion. With the advent of higher frequency 5G bands at FR2 (covering 24.25 to 52.6 GHz) and beyond 5G systems, it is no longer practical to make cabled measurements due to no RF connector reserved for cable testing purposes in the integrated radio transceiver design. As a result, over-the-air (OTA) radiated testing is seen inevitable [2]. Radio channel emulators (CEs), which can physically emulate the radio channel between the transmitter (Tx) and the receiver (Rx), have been widely used for radio performance testing in the laboratory conditions in cabled setup as well as OTA setups [3], [6], [7], [8], [9], [10], [11].

The wireless (virtual) cable solution, which aims to achieve cabled testing functionality (i.e., desired testing signals guided to respective antenna ports with high isolation to other DUT antenna ports) OTA without actual RF cables, has attracted great attention recently both from industry and academia [3], [4], [8], [9], [10], [11], [12], [13], [14], [15], [16], [17], [18], [19], [20], [21]. The main idea is that we can estimate and then calibrate out the unknown transfer matrix between the probe antenna ports and DUT antenna ports, thus enabling guided signal transmission to the respective DUT antenna port via the established virtual cable connection. Several schemes have been proposed in the state-of-the-art works for estimating the unknown transfer matrix, which generally requires information reported by the DUT in active working mode with an active LTE/5G NR connection established between the UE and the BS, for example, with known pilot sequence in [12], and [14], with the reference signal received power (RSRP) measurement per DUT antenna port supporting 2×2 multiple-input multiple-output (MIMO), and the reference signal antenna relative phase (RSARP) among antenna ports

Manuscript received 10 May 2022; revised 5 October 2022; accepted 1 November 2022. Date of publication 15 August 2023; date of current version 6 October 2023. This work was supported in part by the Project European Partnership on Metrology MEWS under Grant 21NRM03, and in part by Huawei Technologies. *(Corresponding author: Wei Fan.)*

Wei Fan is with the National Mobile Communications Research Laboratory, School of Information Science and Engineering, Southeast University, Nanjing 210096, China (e-mail: fwlovethisworld@gmail.com).

Mengting Li and Fengchun Zhang are with the Antenna Propagation and Millimeter-wave Systems (APMS) Section, Aalborg University, 9220 Aalborg, Denmark.

Zhengpeng Wang is with the Department of Electronics and Information Engineering, Beihang University, Beijing 100191, China.

Color versions of one or more figures in this article are available at https://doi.org/10.1109/TAP.2023.3303992.

Digital Object Identifier 10.1109/TAP.2023.3303992

in [15], [16], and [22], and with RSRP value reported per DUT antenna only in [11], and [13], and with maximum RSRP reported for all DUT antenna ports in [23].

The solution based on RSRP-only measurement was later extended to high-order MIMO terminals in [9], and [18]. This wireless cable scheme is highly attractive and has been widely adopted in the industry, e.g., for a 2 × 2 MIMO setup in 39 GHz in [17] and for a 2 × 2 MIMO modem in the automotive scenario in [8], and [10]. State-of-the-art wireless cable schemes are generally implemented with the help of radio CEs. However, the CEs are not customized for such implementations, leading to expensive implementation and waste of valuable digital CE resources, as discussed in this article. As already explained in [9], and [11], the number of probe antennas can be larger than that of the DUT antennas to improve the wireless cable quality, which however, would further increase the system cost significantly with state-of-the-art implementations. The wireless cable solution can be a valuable alternative to the traditional cabled setup for many testing scenarios where a CE is not needed. Furthermore, so far, there has been no general discussion on the relationship among CE resource in terms of interface ports and digital fading channels, number of probe antennas, and number of DUT antennas. We aim to address the above-mentioned challenges in this article.

1) A stand-alone programmable amplitude and phase control solution is proposed to implement the wireless cable scheme, which can save the resource of the CE and thus significantly reduce the system cost.
2) Furthermore, the proposed scheme (with the help of an additional switch matrix) makes it possible to employ more probe antennas without significantly increasing the setup cost.
3) The proposed scheme is experimentally validated both in the vector network analyzer (VNA)-based passive measurement setup as well as in the active measurement setup composed of a commercial 5G BS and a 5G mobile handset supporting 4 × 4 MIMO spatial multiplexing mode, which has not been reported yet in the state-of-the-art works, to the best knowledge of the authors.
4) The proposed scheme can serve as a stand-alone solution that can establish wireless cable connections without CEs, which can be valuable for testing scenarios where channel emulation is not needed.

In Section II, we elaborate on the system model for the wireless cable scheme and current implementations. In Section III, we discuss the proposed implementation scheme. The experiment validations and results in the passive and active measurement setups are discussed in Sections IV and V, respectively. Section VI concludes the work.

II. Problem Statement

A. System Diagram

The cabled setup for MIMO performance testing is shown in Fig. 1 (top) [24]. The signal model can be written as

$$\boldsymbol{y}(f,t) = \boldsymbol{s}(f,t) = \boldsymbol{H}(f,t)\boldsymbol{x}(f,t) + \boldsymbol{n}(f,t) \tag{1}$$

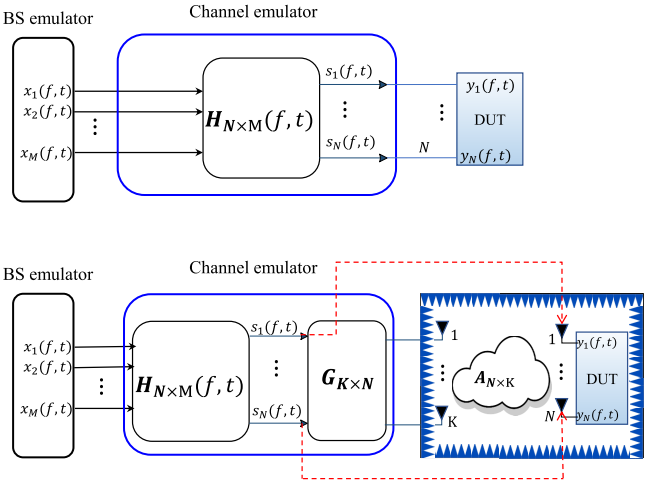

Fig. 1. System diagram for the cabled setup (top) and wireless cable setup (bottom) for a $N \times M$ MIMO systems (with $M \geq N$).

where $\boldsymbol{H}(f,t) \in \mathbb{C}^{N\times M}$ is the wideband time-variant MIMO radio channel model between the M BS antenna ports and the N UE antenna ports (with $M \geq N$). $\boldsymbol{x}(f,t) \in \mathbb{C}^{M\times 1}$, $\boldsymbol{y}(f,t) \in \mathbb{C}^{N\times 1}$, $\boldsymbol{s}(f,t) \in \mathbb{C}^{N\times 1}$, and $\boldsymbol{n}(f,t) \in \mathbb{C}^{N\times 1}$ are the transmit signal vector at the M BS antenna ports, they receive signal vector desired testing signal vector, and noise vector at the N DUT antenna ports, respectively. With the cabled setup, we can assume $\boldsymbol{y}(f,t) = \boldsymbol{s}(f,t)$, i.e., desired testing signal guided to respective DUT antenna port, without any distortion.

The scheme of wireless cable setup is shown in Fig. 1 (bottom), where the system consists of a BS emulator, a radio CE, multiple probe antennas placed in an RF-shielded enclosure, and a DUT. Neglecting noise term at the Rx, the signal model can be written as

$$\boldsymbol{y}(f,t) = \boldsymbol{A}\boldsymbol{G}\boldsymbol{s}(f,t) = \boldsymbol{A}\boldsymbol{G}\boldsymbol{H}(f,t)\boldsymbol{x}(f,t) \tag{2}$$

where $\boldsymbol{A} \in \mathbb{C}^{N\times K}$ and $\boldsymbol{G} \in \mathbb{C}^{K\times N}$ denote the unknown transfer matrix between the K probe antenna ports and N DUT antenna ports, and the calibration matrix, respectively. The number of probe antenna ports K should be no smaller than the number of the DUT antenna ports N (i.e., $K \geq N$). As discussed, the wireless cable connection is established to achieve the same functionality as cabled testing setup, once we can design the calibration matrix $\boldsymbol{G}$ such that $|\boldsymbol{A}\boldsymbol{G}| \approx \boldsymbol{I}_{N\times N}$ can be achieved, with $\boldsymbol{I}_{N\times N} \in \mathbb{R}^{N\times N}$ an identity matrix. The equivalent channel model implemented in the CE is, therefore,

$$\boldsymbol{H}_{\mathrm{CE}}(f,t) = \boldsymbol{G}\boldsymbol{H}(f,t). \tag{3}$$

B. State-of-the-Art Implementation of Calibration Matrix $\boldsymbol{G}$

CE is an essential component in the cabled setup for MIMO performance testing. As shown in Fig. 1 (top), the required CE resource in the cabled setup includes M input interface and N output interface ports, and $N \times M$ digital fading channels for the downlink communication link.

The calibration matrix $\boldsymbol{G}$ is typically implemented with the phase and amplitude tuning networks in the CE output

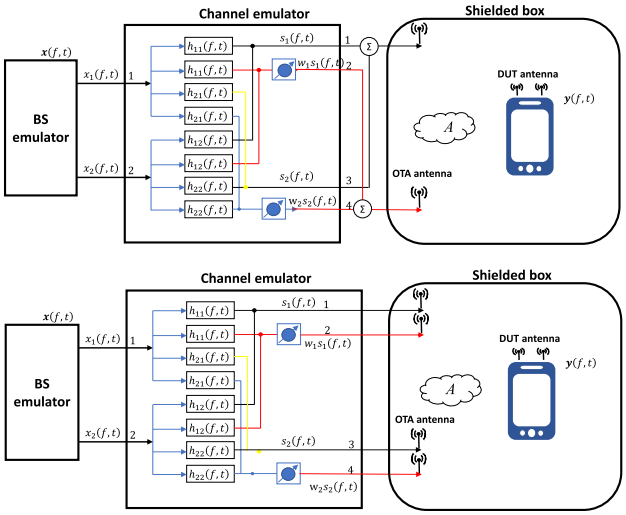

Fig. 2. System diagram for the wireless cable setup for a 2 × 2 MIMO systems with $K = 2$ (top) and $K = 4$ (bottom).

interface ports in the state-of-the-art works. For a wireless cable setup with $K = N$ probe antennas, the required system resource includes a CE with M input interface ports, N^2 output interface ports, $M \times N^2$ digital fading channels and a N-way power splitter [9], [11], [18]. For the nth wireless cable connection to the nth DUT antenna port, we need to tune N phase shifters connected to the N probe antennas such that we can form nulls toward the other $(N-1)$ unintended DUT antenna ports and a peak toward to target nth DUT antenna port, guiding desired testing signal $s_n(f,t)$ to the nth DUT antenna port. Note that the nth column vector of the calibration matrix $\boldsymbol{G} \in \mathbb{C}^{N\times N}$ is designed to establish the nth wireless cable connection. An example is shown in Fig. 2 (top) for a wireless cable setup of a 2 × 2 MIMO device with $K = 2$ [11], where we need a CE of two interface input ports, four interface output ports, and eight digital fading channels, which is more than that in the conventional cabled setup.

An extended implementation is shown in Fig. 2 (bottom), where $K = 4$ probe antennas are employed (with $K > N$). Such implementation will not save the CE resource, as shown in the plot. However, as explained in [11], we have the flexibility to select the optimal routing which offers the best wireless cable quality (i.e., with the lowest cross-talks). The routing matrix divides the four probe antennas into two groups, each of which is responsible for establishing a wireless cable connection. By selecting the optimal combination, we can effectively reduce the likelihood of an unfavorable transfer matrix, although with the cost of longer calibration time for finding the optimal routing (i.e., brute-force search for each routing matrix). As shown in Fig. 2 (bottom), probes 1 and 2 and probes 3 and 4 are grouped for the selected routing scheme. The routing matrix can be implemented with the help of CE due to the flexible channel model settings in the digital baseband in the CE. In our previous work in [23], the main contribution was to achieve wireless cable testing for MIMO terminals based on maximum RSRP measurement, i.e., without the need for RSRP measurement per antenna port. However, its system implementation in [23] would correspond to Fig. 2 (top), i.e., conventional wireless cable implementation which requires extra CE resource.

As discussed in [9], and [11], the quality of the wireless cable connection is determined by the achieved isolation levels among wireless cables. The quality and robustness of the wireless cable are ruled by the condition number of the transfer matrix $\boldsymbol{A}$, which is determined by the probe antenna, multipath propagation within the RF-shielded enclosure, and DUT antennas. The DUT is typically tested as a black box, where the locations and radiation patterns of DUT elements are unknown. The lack of knowledge of DUT and propagation environment makes it infeasible to control the condition number of the matrix $\mathbf{A}$.

Adding more probe antennas can effectively improve the condition number of $\boldsymbol{A}$. With the state-of-the-art implementation with the CE, such scheme will become cost-prohibitive when employing a large number of probe antennas, since the required number of CE output ports is proportional to the square of the number of probe antennas. The problem will also become much more pronounced for high-order MIMO DUTs since N^2 CE output interface ports and $M \times N^2$ digital fading channels in the CE are the minimum requirements with the state-of-the-art wireless cable implementations. As the MIMO order goes up, high-quality wireless cable connections will be more difficult to establish, since more cross-talks should be suppressed. Therefore, employing more probe antennas would become essential to improve the wireless cable quality, which would further increase the setup cost.

As a summary, with state-of-the-art implementations, excessive CE resources (i.e., much higher than in the cabled testing setup) in terms of digital fading channels and output interface ports are required, leading to an expensive system setup. This is mainly due to the fact that the phase and amplitude tuning networks in the CE output interface ports are mainly designed for calibrating RF channels in the CE, which is not customized for implementing the calibration matrix $\boldsymbol{G}$.

III. Proposed Setup and Calibration Procedure

A. Proposed Setup

1) Basic Full-Mesh Setup: In this work, we propose to employ a stand-alone programmable amplitude and phase control network to implement calibration matrix $\boldsymbol{G}$ in the wireless cable setup, thus significantly reducing the system cost and extending the method for other testing scenarios where CE is not required. A system diagram of the proposed setup is shown in Fig. 3. A dedicated programmable amplitude and phase control network with N input ports (connected to the testing instrument ports) and K output ports (with a minimum $K = N$ in the basic setup) (connected to the probe antenna ports) is introduced to implement the calibration matrix $\boldsymbol{G}$, resulting in $N \times K$ phase-amplitude control full-mesh links.

The testing signals s_n for $n \in [1, N]$ can be generated by a genetic testing instrument. That is, such implementation makes it possible to establish wireless cable connections for setups without involving a CE. Note that programmable phase matrix networks have been adopted in the literature to reduce the system cost, e.g., for BS beamforming testing

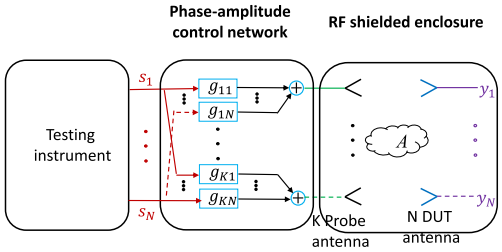

Fig. 3. System diagram for the proposed wireless cable setup with the full-mesh implementation.

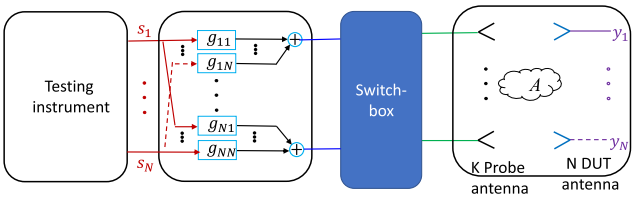

Fig. 4. System diagram for the proposed wireless cable setup with the simplified implementation.

in conductive setup in [25], and [26]. With the proposed method, the key benefit is that the CE resource (if required) can be significantly reduced to be equivalent to that in the cabled setup, compared to state-of-the-art implementations. As explained later, the phase shifters in the calibration stage are tuned to estimate the transfer matrix $\boldsymbol{A}$, and they are needed to implement the inverse of the estimated transfer matrix as well. Therefore, a programmable amplitude and phase control matrix with small least significant bits (LSBs) is desired to reduce quantization errors.

2) Setup With More Probe Antennas: Though cheap, this basic setup (with $K = N$) might suffer from establishing wireless connections with low isolation levels in a specific testing environment, which will become more severe, especially for higher-order MIMO systems. To achieve a given isolation level, it is much more challenging for higher-order MIMO systems. As discussed in Section II and in [9] and [11], a larger number of probes K can effectively improve the condition of the transfer function matrix and thereby enhancing the wireless cable performance. A straightforward solution is to directly set a large K in Fig. 3. With this "full-mesh" strategy, the cost for a phase-amplitude control network (which necessitates $N \times K$ phase-amplitude control links) will increase, especially when a large K is required.

As an alternative, a more cost-effective and simplified setup can be employed by introducing an extra switch matrix, as shown in Fig. 4. The phase and amplitude control matrix can be equipped only with N input and N output ports. A full-connection switch matrix with N input ports and K output ports can help route the signal from the phase and amplitude control network to the K probe antenna ports. A switch network is much cheaper than a high-performance phase and amplitude control network at sub-6 GHz. As discussed later, we need to conduct a calibration procedure before the actual throughput testing, to determine the unknown transfer matrix between the output ports of the phase-amplitude control network and the DUT antenna ports (which includes the switch matrix setup). The responses of the RF chains in the switch matrix are embedded in the measured transfer matrix and will be calibrated out when implementing the calibration matrix $\boldsymbol{G}$. Therefore, it is not necessary to calibrate in advance the switch matrix in the setup. With the proposed setup, the CE resource is independent of the probe antenna number and we can thereby employ many more probe antennas to improve the robustness and quality of the wireless cable in practical setups.

As discussed, the transfer matrix $\boldsymbol{A}$ is unknown and is determined by probe antennas, RF enclosure chamber environment, and DUT antennas. Though the proposed strategy of utilizing more probe antennas can effectively improve the condition number of the transfer matrix for achieving wireless cable implementation, it is unclear what type, polarization, and configuration of probe antennas (e.g., single-polarized or dual-polarized) would be more beneficial in practice. This work regarding probe antennas will be included in future work.

B. Calibration Procedure

The objective is to design and control the amplitude and phase control network such that the testing signal s_n can be guided to the nth DUT port ($n \in [1, N]$), with high isolation (i.e., weak signal leaking) to the other DUT ports. The calibration procedure can be carried out in the setup shown in Fig. 3, as explained below.

1) Amplitude and phase matrix control network calibration. We need to first calibrate the amplitude and phase matrix control network to ensure accurate amplitude and phase setting in each input–output RF chain, which can be done with a network analyzer.
2) Phase matrix tuning and RSRP measurements at the DUT antenna ports. We can enable s_1 from the testing instrument output ports while disabling all other output ports (i.e., $s_n = 0$ for $n \neq 1$). We initially set 0° for all K phase shifters associated with s_1. Then, we toggle the phase term for g_{11} (i.e., the phase shifter between s_1 and the first probe antenna) P times ($P \geq 3$) from 0° to 360° while keeping 0° for all other $K-1$ probe antennas g_{1k} for $k \neq 1$. For each phase setting in the amplitude-phase control network, we record RSRP values at the N DUT antenna ports. We can repeat the same procedure for the other phase terms g_{k1} (i.e., the phase shifter between s_1 and the kth probe antenna) for $k \in [1, K]$. In total, we have $K \times (P-1)+1$ RSRP measurements. Note that we can also activate other testing signals s_n for $n \in [1, N]$, and repeat the same procedure as well, which is equivalent since the transfer matrix is fixed for any testing signal activation.
3) Transfer matrix $\boldsymbol{A}$ estimation. According to [9], the complex transfer matrix $\boldsymbol{A}$ can be estimated based on the above RSRP measurement data, which yields

$$\hat{\boldsymbol{A}}_{N\times K} = \begin{bmatrix} e^{j\phi_1^o} & & \\ & \ddots & \\ & & e^{j\phi_N^o} \end{bmatrix}_{N\times N} \boldsymbol{A}_{N\times K} \qquad (4)$$

where $e^{j\phi_n^o}$ is the unknown phase term for the nth wireless cable for $n \in [1, N]$, which is fixed and irrelevant

to the probe antenna index k. As explained in [9], the relative phase difference among virtual cables, though unknown, will not affect the throughput measurements and achieved isolation among wireless cables. This is the same as in the cabled setup where the phase might be different due to nonidentical RF cables. Therefore, the estimated transfer matrix $\hat{\boldsymbol{A}}$ can be used to calibrate out the $\boldsymbol{A}$ and the wireless cable connections can be effectively established.

4) Calibration matrix $\boldsymbol{G}$ implementation. We can then implement the calibration matrix $\boldsymbol{G} = \hat{\boldsymbol{A}}^{-1}$ (with $()^{-1}$ being the pseudo-inverse operator) in the amplitude and phase control matrix, such that $|\boldsymbol{AG}| \approx \boldsymbol{I}_{N\times N}$ can be achieved.

Once the wireless cable connection is established after performing the calibration, we can perform the actual active testing by establishing the connection between the testing instrument and DUT.

C. Discussions

1) Implementation With More Probe Antennas: As explained, a large K is preferable to improve the quality and robustness of wireless cable implementation in practical setups. The addition of a switch matrix can improve the quality of established wireless cable links by using more probes while reducing the required amplitude and phase control links, compared to the full-mesh configuration. With such implementation, we need to select the optimal subset of N probe antennas out of K probe antennas with the switch matrix, which offers the transfer matrix with the minimum condition number. One straightforward scheme is to select N probe antennas out of K probe antennas in a brute-force manner and measure the corresponding $N \times N$ transfer matrix for each subset, referring to the calibration procedure in Section III-B, which leads to C_K^N subsets of probe antennas following the combination operation of transfer matrices. To simplify the calibration procedure, one probe antenna is taken as a reference antenna and the rest $K-1$ probe antennas are divided into $\lceil (K-1)/(N-1) \rceil$ groups, where $\lceil \rceil$ is the operator rounding up to the nearest integer. The probe antennas in each group together with the reference antenna conducted the calibration procedure. Consequently, in total $\lceil (K-1)/(N-1) \rceil$ calibration procedures are conducted in a nonrepetitive manner. The transfer matrix $\boldsymbol{A}_{N\times K}$ can be reconstructed based on the measurement data and the optimal $N \times N$ transfer matrix can be selected from the matrix $\boldsymbol{A}_{N\times K}$ in a brute-force manner in postprocessing, which determines the optimal subset of N probe antennas out of K probe antennas as well. For example, suppose $K = 4$ and $N = 2$, we only need to perform three calibration procedures, i.e., probes 1 and 2, 1 and 3, and 1 and 4, with probe 1 selected as the reference probe antenna. We can then reconstruct the full $\boldsymbol{A}_{2\times 4}$ matrix in postprocessing.

2) Measurement Uncertainties: Measurement uncertainty is an essential aspect for any OTA method to be standardized [27]. With our proposed wireless cable scheme. The measurement uncertainties can be grouped into several categories.

1) DUT RSRP Reporting Uncertainty. As discussed in [22], and [28], due to the fact that the RSRP reports are not precisely calibrated at the chip level, the reported values may contain errors of ± 2 dB in the RSRP. In addition, the reporting errors with different Rxs may differ. DUT RSRP reporting uncertainties have been discussed in standards, which also apply to our proposed wireless cable scheme.
2) Similar to other MIMO OTA solutions as discussed in [29], we also need to consider the measurement uncertainties in the system instruments, including gNB emulator (e.g., absolute level accuracy, nonlinearity, and frequency characteristic of the gNB emulator), CE (e.g., absolute level accuracy, nonlinearity, frequency characteristic, and stability), power amplifier uncertainties (e.g., stability, linearity, noise figure, mismatch, and gain), and DUT sensitivity drift. These uncertainties are covered in the standardization, which also applies to our proposed scheme.
3) Measurement uncertainties with the phase shifter, attenuator, and switch network. These system components are newly introduced compared to existing OTA solutions. In our work, our key concern is that if the condition number of the transfer matrix between amplitude and phase control network output ports and DUT antenna ports is large. A good isolation level might be unachievable in practical setups due to an ill-conditioned matrix. That is, even small measurement uncertainties associated with the phase shifter and attenuator matrix might be severely amplified. To address this aspect, we performed a Monte-Carlo simulation in the measurement session for the measured transfer matrix (see in Section IV-D) to reflect potential performance deterioration due to the uncertainties introduced by practical phase shifters and attenuator.

3) Advantages of the Proposed Setups: The proposed wireless cable implementation scheme is highly attractive for OTA radiated testing, due to several reasons. The whole measurement can be performed with the DUT placed in a compact and shielded anechoic box in the near-field of the probe antennas, which implies that the setup can be cost-effective, movable, and flexible. This is advantageous compared to the standard multiprobe anechoic chamber (MPAC) and radiated-two-stage (RTS) solution where a large anechoic chamber is typically required. Furthermore, the calibration measurements can be performed in a fast and automated manner (in the order of seconds) even for high-order MIMO radios. It is a generic solution that works for most MIMO radio specifications, e.g., WiFi, cellular terminals, BSs, automotive communication systems, due to the fact that RSRP value per DUT antenna port is generally accessible.

The calibration procedure and actual performance measurements can be done in a fully automatic manner, since the DUT stays untouched, which implies that there is no need for operators to intervene. It works for radio devices of any MIMO order without significantly increasing the calibration complexity, as demonstrated in [9]. It supports emulation of arbitrary MIMO channel models, including 3-D and dynamic

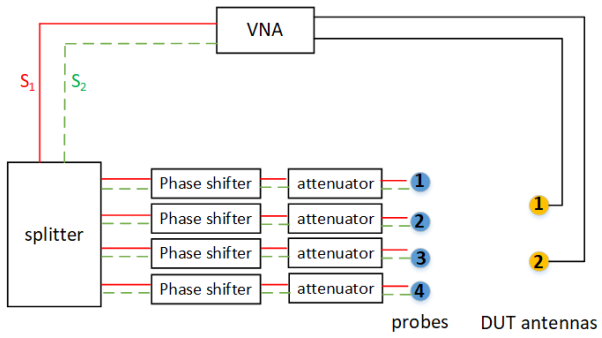

Fig. 5. Diagram of the VNA-based passive measurement system.

Fig. 6. Photograph of the measurement system.

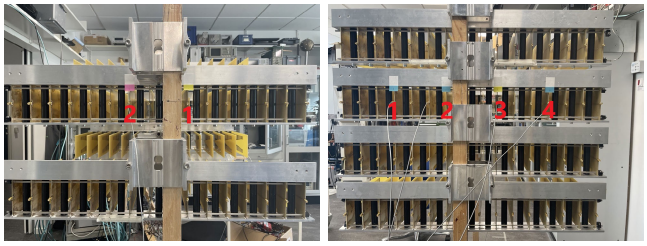

(a) (b)

Fig. 7. Photographs of (a) DUT and (b) probe antennas.

spatial channel models. It only requires a short calibration time to retrieve the transfer matrix (i.e., in the order of seconds) with the proposed closed-form calibration scheme in [9].

As discussed, compared to state-of-the-art wireless cable implementations with the help of CE, the proposed scheme can significantly reduce the system cost, making the cost comparable to the traditional cabled solution, by introducing off-the-shelf amplitude-phase control network and switching network. The proposed scheme can be adopted to achieve wireless cable connections, with or without radio CEs, which makes the solution more generic.

One potential downside of the proposed scheme is that the external phase and amplitude network, switch matrix, and OTA transmission in the RF-shielded enclosure would introduce link budget issues due to the loss. The measurement accuracy would be affected by the limited system dynamic range. The wireless cable concept is to create balanced, highly isolated wireless cable links, while the signaling condition for the achieved wireless cable is not taken into consideration. Therefore, the absolute power might be problematic for the achieved wireless cable. In practice, power amplifiers might become essential to meet the requirement of good signal levels in active throughput measurements.

IV. VNA-Based Passive Measurements

In this section, we validate wireless cable performance both with the full-mesh and switch matrix schemes in the VNA-based passive measurement setup. Active throughput measurements with a real 5G BS and a commercial mobile handset will be discussed later in Section V.

A. Measurement System

An illustration of the VNA-based passive measurement setup and a photograph of the measurement system is shown in Figs. 5 and 6, respectively. The details of the devices used in the measurement campaign are given as follows.

1) A VNA.
2) Four digital attenuators with a step size of 0.1 dB and an attenuation range of 90 dB.
3) Two identical 1×16 vertically polarized modified Vivaldi antenna arrays, one for the probe antenna array (with four elements selected) and the other for the DUT antenna array (with two elements selected). The dimensions of the antenna unit are 30×10 cm with a gain of around 9 dBi at 3 GHz.
4) Four digital phase shifters with a phase adjustment range of 360° and phase adjustment resolution of 1°.
5) One 1-to-4 power splitter.
6) A laptop which controls the digital phase shifters, and digital attenuators and communicates with VNA to save the recorded data.

The passive measurements employ two DUT antennas and four probe antennas, which are selected from two identical 1×16 uniform linear arrays, respectively, as shown in Fig. 7. Since two DUT antennas are employed in our passive measurements, we are supposed to establish two wireless cable links for two transmitting signals, i.e., s_1 and s_2 as shown in Figs. 3 and 4 (with two spatial streams). In our passive measurements, two wireless cable links are established successively. That is, we first validate the first wireless cable link via setting the first column of the compensation matrix with the amplitude and phase control network, which aims to guide s_1 to the DUT antenna 1 while avoiding much leakage of s_1 to the DUT antenna 2, and then repeat it for validating the second wireless cable link (with a new set of amplitude and phase settings in the amplitude and phase control network), as shown in Fig. 5. The measurements were conducted in a typical indoor laboratory scenario. The signals generated by the VNA were split by the power divider, delivered to the modulated digital phase shifters and attenuator, then transmitted by probe antennas, and finally received by DUT antennas. The power of the signals received by DUT antennas is taken as the measured RSRPs in these passive measurements. Note that the switch matrix used in the switch matrix setup is implemented by manually disconnecting the unselected probes.

The probes and the DUT are aligned with each other with a face-to-face distance of around 11 cm. The probe

antennas and DUT antennas have the same element spacing of 150 mm and their indices can be seen in Fig. 7. The first and second elements of the DUT are aligned face-to-face with the second and third of the probe antenna, respectively. The measurement data were recorded by VNA from 2.95 to 3.05 GHz with 2001 frequency samples. Note that the phase shifters and the attenuator are not ideal in practice, where uncertainties introduced by phase shifters and attenuator are within ± 0.4 dB and $\pm 2.5^\circ$ according to the manufacture specifications, respectively.

B. Calibration Measurement Procedure

As mentioned before, the matrix $\boldsymbol{A}$ should be estimated in the calibration procedure to establish the wireless cable. Therefore, the main objective of the calibration procedure is to determine the unknown transfer matrix between the output ports of the phase-amplitude control network and the DUT antenna ports. For the setup with a switch matrix in Fig. 4, the responses of the chains of the switch matrix are embedded in the measured transfer matrix and will be calibrated out when implementing the calibration matrix $\boldsymbol{G}$. We do not need to calibrate the switch matrix in the setup in Fig. 4, as long as it is stable and the relative differences among chains remain unchanged during testing. In our measurements, the matrix $\boldsymbol{A}$ is obtained via applying the method proposed in [9]. Hence, the measurement procedure is only outlined as follows.

1) All of the phase shifters are initially set to 0° and the power of the signal received by the first DUT antenna is recorded by the VNA. Tune the phase shifter connected with the first probe antenna to two states, i.e., 90° and 180°, respectively, while keeping 0° phase setting for the rest of probe antennas. For each phase setting, the power of the signal received by the first DUT antenna is recorded by the VNA. This phase tuning measurements are repeated for the rest of the probe antennas.
2) Repeat the above measurements and record the power of the signals received by the second DUT antenna.

Note that the two steps can be combined and carried out simultaneously if we use a three-port VNA. Based on the 18 power measurement data, the transfer matrix $\boldsymbol{A}_{2\times 4}$ can be solved according to [9].

C. Wireless Cable Evaluation Measurement

The validation measurements for full-mesh and switch matrix setups are performed as detailed below.

1) Full-Mesh Setup: Once the transfer matrix $\boldsymbol{A}_{2\times 4}$ has been estimated, the calibration matrix $\boldsymbol{G}_{4\times 2} = \boldsymbol{A}_{2\times 4}^{-1}$ can be calculated and implemented with the phase-amplitude control network to establish the wireless cable connections. To evaluate the quality of the nth wireless cable connection, the nth column vector of $\boldsymbol{G}_{4\times 2}$ is implemented and the power values at both DUT antennas are recorded, which yields the corresponding isolation level.

2) Switch Matrix Setup: Based on the estimated transfer matrix $\boldsymbol{A}_{2\times 4}$, we can select any two column vectors from $\boldsymbol{A}_{2\times 4}$ to form a transfer matrix for the given subset of probes denoted by $\tilde{\boldsymbol{A}}_{2\times 2}$ and calculate the condition number of it, in the brute-force manner. In this validation measurement, all of the two-probe subsets are implemented to establish the wireless cable connections. For a given subset, the calibration matrix $\boldsymbol{G}_{2\times 2} = \tilde{\boldsymbol{A}}_{2\times 2}^{-1}$ is calculated. To evaluate the nth wireless cable connection, the splitter is only connected with the selected probe antennas, and the nth column vector of $\boldsymbol{G}$ is implemented with the corresponding phase and amplitude links. The power values at both DUT antennas are then recorded, resulting in the isolation level of the nth wireless cable connection for the given subset. In this way, we can obtain the isolation levels of both wireless cable connections for all of the two-probe subsets.

D. Measurement Results

1) Monte-Carlo Simulations: Monte-Carlo simulation is used to demonstrate the impact of the uncertainties of the phase shifters and the attenuators on the achieved performance of the wireless cable. We measured the realistic transfer matrix for a specific measurement scenario and investigate the impact of phase and amplitude control uncertainties on the wireless cable performance. With an ill-conditioned transfer matrix, even a small error can be significantly amplified, leading to unreliable results. Both the phase shifter and the attenuator present quantization/stepping errors and uncertainties in both amplitude and phase. As explained, we need to tune the phase shifter in the calibration stage to estimate the unknown transfer matrix, and we also need to set the phase shifter and attenuator in the control network to implement the inverse of the estimated transfer matrix. Therefore, the implementation errors introduced by the phase shifters and the attenuators are unavoidable in practice due to the quantization error. We can in principle employ a phase shifter and digital attenuator with a small LSB to reduce the quantization error. In addition, amplitude and phase might drift as well due to time and environment. We thereby run Monte-Carlo simulations with 500 realizations based on the estimated transfer matrix $\boldsymbol{A}_{2\times 4}$ for the full-mesh setup and the selected matrices $\tilde{\boldsymbol{A}}_{2\times 2}$ for the switch matrix setup. The corresponding calibration matrix $\boldsymbol{G}_{4\times 2} = \boldsymbol{A}_{2\times 4}^{-1}$ and $\boldsymbol{G}_{2\times 2} = \tilde{\boldsymbol{A}}_{2\times 2}^{-1}$ are assumed implemented with the 8-bit phase shifters with the uncertainties of ± 0.25 dB in amplitude and $\pm 2.5^\circ$ in phase and the attenuators with 0.1 dB step-size in the case with 40 dB signal-to-noise (SNR) ratio. For each setup in each realization, we calculate the corresponding isolation levels for both wireless cable connections and select the lower isolation level to evaluate the performance of the wireless cable connections. A cumulative distribution function based on the isolation level data is introduced to statistically evaluate the performance of the wireless cable connections, as shown in Fig. 8. It shows that the transfer matrices of the two subsets with the largest condition numbers, i.e., 1 and 3 and 2 and 4, perform worst as expected, where only up to 50% realizations can achieve an isolation level $\geq$20 dB, comparing to other configurations with more than 95% realizations. The curves demonstrate that the configuration, whose transfer matrix with the lowest condition number, can most likely achieve the highest isolation level, i.e., the best wireless cable connections.

2) Measured Isolation Levels: The condition numbers of the matrices and the measured isolation levels for the full-mesh setup and the switch matrix setup, are summarized in Table I. It shows that the condition number of matrix $\boldsymbol{A}_{2\times 4}$ is 1.2 and

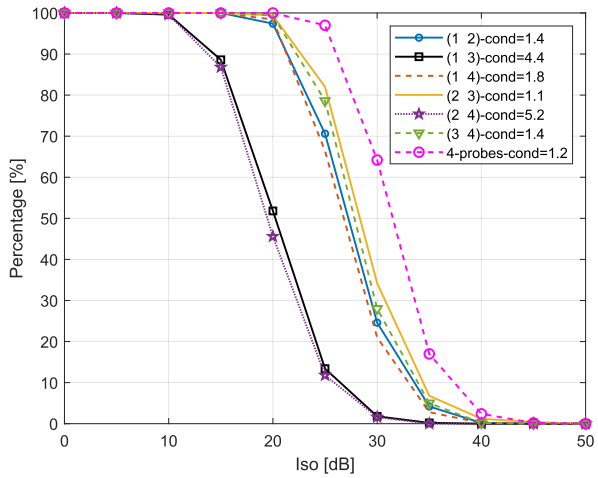

Fig. 8. Cumulative curves of the isolation levels achieved by different setups.

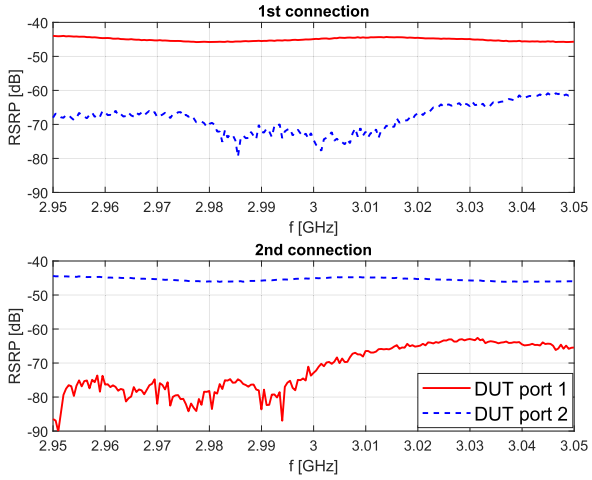

Fig. 9. RSRP curves over 100 MHz for the subset composed of the second and third probe antenna in the cost-effective setup.

TABLE I

CONDITION NUMBER OF THE TRANSFER MATRICES AND ACHIEVED ISOLATION LEVELS

Selected probe index	Condition number of $\mathbf{A}_{2\times4}$ or $\tilde{\mathbf{A}}_{2\times2}$	Isolation level of 1st / 2nd connection [dB]
1 & 2	1.5	34.3 / 20.1
1 & 3	4.4	22.7 / 15.8
1 & 4	1.8	29.8 / 15.3
2 & 3	1.1	28.0 / 25.9
2 & 4	5.2	21.3 / 20.6
3 & 4	1.4	34.0 / 25.4
1, 2, 3 & 4	1.2	28.6 / 30.5

those of the subsets in the switch matrix-based setup vary from 1.1 to 5.2. It can be observed that higher isolation levels can generally be achieved by the configuration with a lower condition number as expected.

The measured RSRP curves over 100 MHz bandwidth for the best subset (composed of the second and thirrd probe antennas) and the worst subset (composed of the second and fourth probe antennas) in the cost-effective setup are shown in Figs. 9 and 10, respectively. Figs. 9 and 10 (top) show the RSRP curves received by both of the DUT antennas when the first wireless cable connection is established while the bottom ones when the second wireless cable connection is established. Figs. 9 and 10 (top) show that the RSRPs received at the first DUT antenna are much larger than that at the second DUT antenna when establishing the first wireless cable connection, and vise versa for the second wireless cable connection in Figs. 9 and 10 (bottom), indicating that the wireless cable connections are well established with the testing signal delivered to the target DUT antenna with only weak leakage to the other DUT antenna. Comparing the qualities of the wireless cable connections in Figs. 9 and 10, higher isolation levels over the whole bandwidth can be achieved with the best subset than those with the worst subset, demonstrating that the smaller condition number of the transfer matrix is essential for establishing more robust wireless cable connections over frequency bands.

As discussed in Section III-C, the subset in the cost-effective setup, which offers the transfer matrix with the minimum condition number denoted by $\tilde{\boldsymbol{A}}_o$, is the optimal

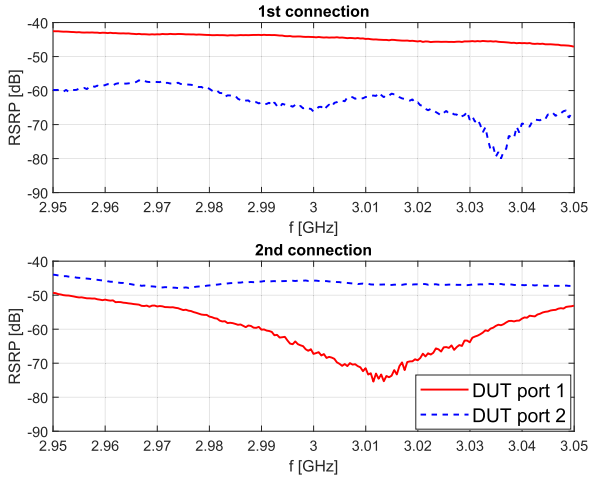

Fig. 10. RSRP curves over 100 MHz for the subset composed of the second and fourth probe antenna in the cost-effective setup.

subset and will be selected to establish the wireless cable connections in practice. Accordingly, the subset composed of the second and the third probe antenna is the optimal subset in this measurement setup, which yields the transfer matrix with the minimum condition number of 1.1 and achieves the isolation levels of 28.0 and 25.9 dB for the two wireless cable connections, respectively. In a practical wireless cable testing, the calibration matrix $\boldsymbol{G} = \tilde{\boldsymbol{A}}_o^{-1}$ will be implemented with the phase and amplitude network while the corresponding probe antennas will be selected with the switch box to establish the wireless cable connections. For the full-mesh setup, the calibration matrix $\boldsymbol{G} = \boldsymbol{A}_{2\times4}^{-1}$ will be directly implemented with the phase and amplitude control network. The established wireless cable connections can achieve isolation levels of 28.6 and 30.5 dB, respectively. The excellent results achieved with both the full-mesh setup and the cost-effective setup demonstrate the effectiveness of the proposed wireless cable solutions.

V. ACTIVE THROUGHPUT MEASUREMENTS

Besides the validation with VNA-based passive measurements presented in Section IV, active throughput measurements with a real 5G BS and a commercial mobile handset

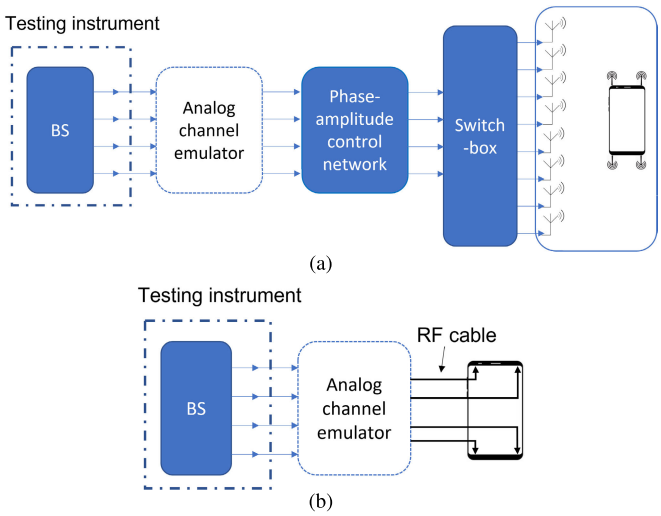

Fig. 11. Diagram of the measurement system for (a) proposed wireless cable setup and (b) conventional cabled conducted setup.

supporting 4 × 4 MIMO spatial multiplexing mode were performed. To the best of our knowledge, this is the first time that active throughput results have been reported for high-order MIMO terminals with the wireless cable scheme. For simplicity, only the switch matrix setup was considered in the active throughput validation measurements. The conventional cabled conducted testing measurement campaign was performed as a reference.

A. Measurement System

The diagram of the measurement system is shown in Fig. 11, which is composed of the real commercial BS, phase and amplitude control network, power amplifiers (to compensate for the signal loss and meet the requirement of signal levels in the throughput measurement, not shown in the diagram), shielded RF enclosure, multiple probe antennas, a commercial mobile handset as the DUT and a computer to collect RSRP values from the DUT antenna ports via the USB cable (not shown in the diagram). Photographs of the BS and DUT in the RF-shielded anechoic enclosure are shown in Fig. 12. The analog channel emulation network composed of power splitters, combiners, and RF cables (as detailed later) is employed to emulate a static MIMO channel matrix with different channel ranks. It is introduced to demonstrate the impact of MIMO channel models on throughput results. The analog channel emulation network is introduced after achieving the wireless cable connection in the active throughput measurement parts, as discussed later. Note that the wireless cable is only implemented for the downlink transmission, while the uplink is realized simply by connecting the communication antennas in the RF-shielded enclosure to the BS antenna ports. The detailed settings of the components in the measurement system are given in Table II.

B. Calibration

As discussed, the first step is to estimate the transfer matrix $\boldsymbol{A}$ among the four selected probe antenna ports and four DUT antenna ports. The calibration procedure discussed in Section III-B is employed here for the calibration procedure.

(a) (b)

Fig. 12. Photographs of the measurement system: (a) 5G BS and (b) RF-shielded enclosure and DUT.

TABLE II
SYSTEM COMPONENTS AND SETTINGS FOR ACTIVE THROUGHPUT MEASUREMENTS

System component	Settings
BS	• Model: Huawei BS with 64 active antenna units (antenna units removed in the cabled setup) and 4 output ports • Frequency band: N78 at 3.5 GHz with 100 MHz bandwidth • Frame structure: TDD duplex mode (DDDDDDDSUUS=8:2:2) • Modulation and coding scheme (MCS) index: adaptive modulation and coding (AMC): 0-28
Phase and amplitude control matrix	• Phase tuning range : 0-360° with 2.8° step • Amplitude tuning range: 0-60 dB with 0.5 dB step • 4 input ports and 4 output ports with full-mesh configuration
RF shielded enclosure and probe antenna	• Model: ETS-Lindgren's 5230 Tabletop RF Test Enclosures • Probe antenna: eight dual-polarized wideband antennas (16 antenna ports) covering 2.5 GHz to 5.5 GHz frequency band. • Eight output ports of the phase and amplitude network is connected to 2 vertically and 2 horizontally-polarized ports of the four lower antennas, and 2 vertically and 2 horizontally-polarized ports of the four upper antennas. Only four probe antenna ports are selected.
DUT	• Huawei mobile phone supporting 4×4 MIMO with Kirin 9000 chipset.

Note that the instability of the RSRP measurement is mitigated by averaging RSRP measurements over time, where 300 ms was set to record the RSRP values. Once the transfer matrix $\boldsymbol{A}$ is estimated with the calibration procedure, we can implement $\boldsymbol{A}^{-1}$ with the phase and amplitude control matrix. The achieved isolation for the four wireless cable connections is shown in Table III, where a minimum of 21.6 dB isolation level can be achieved, indicating the effectiveness of the proposed cost-effective scheme. The achieved isolation level is sufficient to establish a good wireless cable connection for throughput measurement [11].

After the calibration procedure, four wireless cable connections are established. The wireless cable connections will be

TABLE III

ACHIEVED ISOLATION FOR ESTABLISHED WIRELESS CABLE LINKS

Isolation (dB)			
1^{st} link	2^{nd} link	3^{rd} link	4^{th} link
22.9	28.5	21.6	29.4

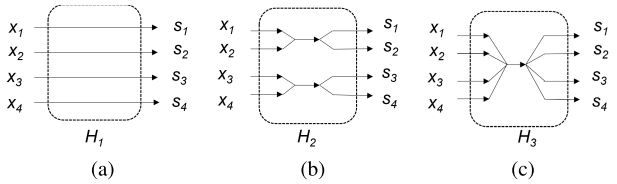

Fig. 13. Diagram of the analog channel emulation network for (a) H_1, (b) H_2, and (c) H_3, respectively.

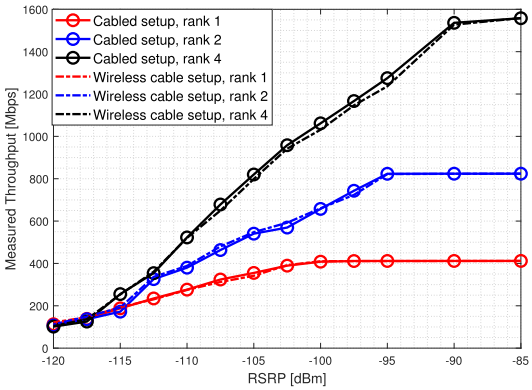

Fig. 14. Measured throughput results for the cabled and wireless cable setups for the three-channel models.

maintained during the active throughput measurement, as long as the amplitude and phase control network, the RF enclosure, and the DUT are untouched.

C. Active Throughput Results

1) Channel Models Implementation: We can perform the MIMO throughput performance testing under arbitrary channel conditions, once a good wireless cable connection is achieved. As discussed, different channel models are realized with an "analog" channel emulation network for simplicity after achieving the wireless cable connections. Three representative static "channel models" are implemented as shown in Fig. 13. The three-channel matrices implemented with the "analog CE," assuming homogeneous RF links are given by

$$H_1 = \begin{bmatrix} 1 & 0 & 0 & 0 \\ 0 & 1 & 0 & 0 \\ 0 & 0 & 1 & 0 \\ 0 & 0 & 0 & 1 \end{bmatrix}, \quad H_2 = \begin{bmatrix} 1 & 1 & 0 & 0 \\ 1 & 1 & 0 & 0 \\ 0 & 0 & 1 & 1 \\ 0 & 0 & 1 & 1 \end{bmatrix}$$

$$H_3 = \begin{bmatrix} 1 & 1 & 1 & 1 \\ 1 & 1 & 1 & 1 \\ 1 & 1 & 1 & 1 \\ 1 & 1 & 1 & 1 \end{bmatrix}. \tag{5}$$

The rank of H_1, H_2, and H_3 is 4, 2, and 1, respectively.

2) Measured Active Throughput Results: The measured throughput results for the conducted and wireless cable setups for the three-channel models are shown in Fig. 14. We have the following observations.

1) The measured throughput increases as the SNR goes up, as expected. A measured downlink peak throughput can be achieved with RSRP -85 dBm for all cases.
2) The measured peak throughput is around 410, 820, and 1560 Mbps for channels with ranks 1, 2, and 4, respectively, whose relationship is in good agreement with its MIMO channel order, as expected.
3) A good agreement of measured throughput results can be observed for the wireless cable and conducted cable setups for all the considered channels [with the best scenario (i.e., full rank with good channel condition number) and the worst scenario (with rank one channel model)].

The measured results clearly validate our proposed cost-effective wireless cable implementation.

VI. CONCLUSION

In this work, state-of-the-art implementations of wireless cable scheme with the help of CE is first revisited. We then highlight that the current implementation requires excessive CE resources in terms of digital channels and output interface ports, making it expensive and inapplicable for high-order MIMO DUT testing. We propose to estimate and implement the calibration matrix using a stand-alone programmable amplitude and phase control matrix, enabling a simple and cost-effective wireless cable implementation. The proposed scheme is highly valuable, as it can significantly reduce the resource requirement of the radio CE. By further introducing the switch matrix network, the proposed scheme is also suitable for high-order MIMO testing with large amounts of probe antennas. The proposed wireless cable scheme also works for test cases where CEs are not required. The proposed scheme is implemented and validated in a practical VNA-based passive measurement setup with $K = 4$ probe antennas and $N = 2$ DUT antennas, and isolation of more than 28.5 and 25 dB can be achieved for the proposed full-mesh and switch matrix implementation, respectively, which demonstrates the robustness and effectiveness of the proposed scheme. Moreover, for the first time, we validated the wireless cable concept for 4×4 MIMO with the proposed scheme in an active measurement setup composed of a commercial 5G BS and a commercial 5G mobile handset, where an isolation of minimum 21.6 dB can be achieved. An excellent agreement of the measured throughput results can be observed for the wireless cable and conducted cable setups for all considered channel models. The throughput measurements in the active setup clearly validate our proposed cost-effective wireless cable scheme.

REFERENCES

[1] M. Shafi et al., "5G: A tutorial overview of standards, trials, challenges, deployment, and practice," *IEEE J. Sel. Areas Commun.*, vol. 35, no. 6, pp. 1201–1221, Jun. 2017.

[2] H. Kong, Z. Wen, Y. Jing, and M. Yau, "Midfield over-the-air test: A new OTA RF performance test method for 5G massive MIMO devices," *IEEE Trans. Microw. Theory Techn.*, vol. 67, no. 7, pp. 2873–2883, Jul. 2019.

[3] H. Gao et al., "Over-the-air performance testing of 5G new radio user equipment: Standardization and challenges," *IEEE Commun. Standards Mag.*, vol. 6, no. 2, pp. 71–78, Jun. 2022.

[4] *New Radio Study on Test Methods*, document 3GPP 38.810, 3GPP, 2022.

[5] *Test Plan for* 2×2 *Downlink MIMO and Transmit Diversity Over-the-Air Performance Version 1.1.1*, CTIA, Washington, DC, USA, 2018.

[6] M. Hofer et al., "Real-time geometry-based wireless channel emulation," *IEEE Trans. Veh. Technol.*, vol. 68, no. 2, pp. 1631–1645, Feb. 2019.

[7] W. Fan, P. Kyösti, L. Hentilä, and G. F. Pedersen, "A flexible millimeter-wave radio channel emulator design with experimental validations," *IEEE Trans. Antennas Propag.*, vol. 66, no. 11, pp. 6446–6451, Nov. 2018.

[8] Y. Ji et al., "Virtual drive testing over-the-air for vehicular communications," *IEEE Trans. Veh. Technol.*, vol. 69, no. 2, pp. 1203–1213, Feb. 2020.

[9] F. Zhang, W. Fan, and Z. Wang, "Achieving wireless cable testing of high-order MIMO devices with a novel closed-form calibration method," *IEEE Trans. Antennas Propag.*, vol. 69, no. 1, pp. 478–487, Jan. 2021.

[10] C. S. P. Lötbäck, K. Karlsson, M. S. Kildal, A. Haliti, M. Nilsson, and R. Iustin, "Evaluation of complete vehicle over-the-air verification methods for multiple-input multiple-output communication systems," in *Proc. 15th Eur. Conf. Antennas Propag. (EuCAP)*, Mar. 2021, pp. 1–5.

[11] W. Fan, P. Kyösti, L. Hentilä, and G. F. Pedersen, "MIMO terminal performance evaluation with a novel wireless cable method," *IEEE Trans. Antennas Propag.*, vol. 65, no. 9, pp. 4803–4814, Sep. 2017.

[12] C. Schirmer, M. Lorenz, W. A. Th. Kotterman, R. Perthold, M. H. Landmann, and G. D. Galdo, "MIMO over-the-air testing for electrically large objects in non-anechoic environments," in *Proc. 10th Eur. Conf. Antennas Propag. (EuCAP)*, Apr. 2016, pp. 1–6.

[13] P. Kyosti, L. Hentila, J. Kyrolainen, and V. T. P. Heino, "Systems and methods for calibrating multiple input, multiple output (MIMO) test systems and for using the calibrated MIMO test systems to test mobile devices," U.S. Patent 9 742 508, Aug. 22, 2017.

[14] P. Kyosti and J. Kyrolainen, "Systems and methods for radio channel emulation of a multiple input multiple output (MIMO) wireless link," U.S. Patent 10 601 695, Mar. 24, 2020.

[15] W. Yu, Y. Qi, K. Liu, Y. Xu, and J. Fan, "Radiated two-stage method for LTE MIMO user equipment performance evaluation," *IEEE Trans. Electromagn. Compat.*, vol. 56, no. 6, pp. 1691–1696, Dec. 2014.

[16] Y. Jing, H. Kong, and M. Rumney, "MIMO OTA test for a mobile station performance evaluation," *IEEE Instrum. Meas. Mag.*, vol. 19, no. 3, pp. 43–50, Jun. 2016.

[17] T. Eichler, U. Philipp, H. Mellein, and L. Rädler, "Virtual cable calibration for OTA testing of 5G mmWave devices," *Microw. J.*, vol. 64, no. 5, pp. 70–78, 2021.

[18] W. Fan, F. Zhang, P. Kyösti, L. Hentilä, and G. F. Pedersen, "Wireless cable method for high-order MIMO terminals based on particle swarm optimization algorithm," *IEEE Trans. Antennas Propag.*, vol. 66, no. 10, pp. 5536–5545, Oct. 2018.

[19] P. Shen, Y. Qi, W. Yu, and F. Li, "Inverse matrix autosearch technique for the RTS MIMO OTA test," *IEEE Trans. Electromagn. Compat.*, vol. 63, no. 4, pp. 962–969, Aug. 2021.

[20] P. Shen, Y. Qi, W. Yu, J. L. Drewniak, M. Yu, and F. Li, "An RTS-based near-field MIMO measurement solution—A step toward 5G," *IEEE Trans. Microw. Theory Techn.*, vol. 67, no. 7, pp. 2884–2893, Jul. 2019.

[21] P. Shen, Y. Qi, W. Yu, J. Fan, Z. Yang, and S. Wu, "A decomposition method for MIMO OTA performance evaluation," *IEEE Trans. Veh. Technol.*, vol. 67, no. 9, pp. 8184–8191, Sep. 2018.

[22] *User Equipment (UE) Antenna Test Function Definition for Two-Stage Multiple Input Multiple Output (MIMO) Over the Air (OTA) Test Method*, 3GPP TR 36.978, Version 13.1.0, 3GPP, 2022.

[23] F. Zhang, M. Li, X. Zhang, Z. Wang, and W. Fan, "Achieving wireless cable testing for MIMO terminals based on maximum RSRP measurement," *IEEE Trans. Antennas Propag.*, vol. 70, no. 8, pp. 7084–7093, Aug. 2022.

[24] *Testing LTE-Advanced (Rel. 10) Application Note*, Rohde & Schwarz, Munich, Germany, 2022.

[25] P. Kyösti and P. Heino, "Fading channel emulation for massive MIMO testing using a conductive phase matrix setup," in *Proc. 14th Eur. Conf. Antennas Propag. (EuCAP)*, Mar. 2020, pp. 1–4.

[26] D. Reed, A. Rodríguez-Herrera, and J.-P. Nuutinen, "Massive MIMO array testing using a programmable phase matrix and channel emulator," in *Proc. 12th Eur. Conf. Antennas Propag. (EuCAP)*, Apr. 2018, pp. 1–4.

[27] *New Radio Derivation of Test Tolerances and Measurement Uncertainty for User Equipment (UE) Conformance Test Cases*, document 3GPP TR 38.903 version 15.4.0 Release 15, 2022.

[28] P. Shen, Y. Qi, W. Yu, J. Fan, and F. Li, "OTA measurement for IoT wireless device performance evaluation: Challenges and solutions," *IEEE Internet Things J.*, vol. 6, no. 1, pp. 1223–1237, Feb. 2019.

[29] *Study on Radiated Metrics and Test Methodology for the Verification of Multi-Antenna Reception Performance of NR User Equipment (UE)*, document 3GPP TR 38.827 V16.8.0, 2022.

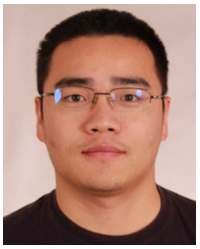

Wei Fan (Senior Member, IEEE) received the B.E. degree from the Harbin Institute of Technology, Harbin, China, in 2009, the double master's degree (Hons.) from the Politecnico di Torino, Turin, Italy, and the Grenoble Institute of Technology, Grenoble, France, in 2011, and the Ph.D. degree from Aalborg University, Aalborg, Denmark, in 2014.

He was with Aalborg University, where he became an Assistant Professor in 2014, a tenured Associate Professor and a Leader of "wireless propagation and over-the-air (OTA) testing" research group in 2017, and a Professor (promotion program) in 2023. He was with Intel Mobile Communications, Denmark, in 2011 and with Anite Telecoms Oy (now Keysight technologies), Finland, in 2014 as a research intern. He has also been holds a Docentship (adjunct professor) with Oulu University, Finland, since 2023. He is a Professor with Southeast University, China. His current research interests include over-the-air (OTA) testing of multiple antenna systems, radio channel sounding, parameter estimation, modeling, and emulation, array signal processing.

Dr. Fan is a senior member of AMTA and URSI, and a Fellow of IET. He was the recipient of the Sapere Aude research talent award from Independent Research Fund Denmark, URSI Young Scientist Award (twice), PIERS young scientist award, IEEE AP-S Young Professional Ambassador, and an unrestricted research gift award from Meta platforms, USA.

Mengting Li received the B.Sc. degree in information engineering and the M.Sc. degree in electronic science and technology from Xi'an Jiaotong University, Xi'an, China, in 2017 and 2020, respectively. She is currently pursuing the Ph.D. degree with the Department of Electronics Systems, Aalborg University.

Her research interests include channel characterization, antenna arrays and antenna diagnosis.

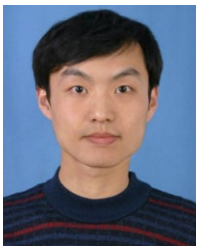

Zhengpeng Wang (Member, IEEE) was born in Shandong, China, in 1981. He received the B.Sc. degree in electronic science and technology from Shandong University, Jinan, China, in 2004, and the M.Sc. and Ph.D. degrees in electromagnetic field and microwave technology from Beihang University, Beijing, China, in 2007 and 2012, respectively.

He was a Visiting Researcher with the Antenna and Applied Electromagnetic Laboratory, University of Birmingham, Birmingham, U.K., in 2009 and 2010. From 2013 to 2015, he was a Research Fellow with the University of Kent, Canterbury, U.K., and the University of Science and Technology Beijing, Beijing, China. He is currently an Associate Professor with Beihang University. His current research interests include reconfigurable filters, reconfigurable antennas, filtering antennas, feed antennas, and 5G OTA measurement.

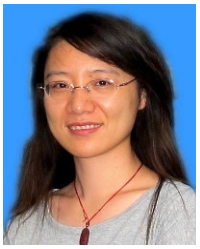

Fengchun Zhang received the B.Sc. degree in optical information science and technology, the M.Sc. degree in acoustics from the South China University of Technology, Guangzhou, China, in 2006 and 2009, respectively, and the Ph.D. degree from Aalborg University, Denmark, in 2019. She is currently an Assistant Professor with the Department of Electronics Systems, Aalborg University. Her research interests are in antenna array signal processing, beamforming, parameter estimation for channel characterization of centimeter and millimeter wave wireless systems, and over the air testing.